

EXPERIMENTAL TECHNIQUES TO STUDY THE COMBUSTION OF AQUEOUS
SOLUTIONS OF HYDROXYLAMMONIUM NITRATE WITH ADDITIVES

A Thesis

by

GABRIEL DYLAN HOMAN-CRUZ

Submitted to the Office of Graduate and Professional Studies of
Texas A&M University
in partial fulfillment of the requirements for the degree of

MASTER OF SCIENCE

Chair of Committee,	Eric Petersen
Committee Members,	Timothy Jacobs
	Adonios Karpetis
Head of Department,	Andreas Polycarpou

December 2015

Major Subject: Mechanical Engineering

Copyright 2015 Gabriel Dylan Homan-Cruz

ABSTRACT

Aqueous solutions of hydroxylammonium nitrate (HAN) are promising as possible replacements for hydrazine as liquid rocket propellants. HAN-based propellants offer lower toxicity, higher density, and possibly higher specific impulse compared to hydrazine, but further research is needed to fully understand the combustion of HAN mixtures and to implement them in actual applications. The thesis presented here studies the combustion of HAN mixtures in a constant volume strand-burner over a pressure range between 3 and 20 MPa.

A solution of 82.4 wt% HAN in water was used as a baseline from which other solutions were created. Silica and titania nanoparticles were added separately at concentrations of 1 wt% and 3 wt% in the baseline solution based on previous studies that have shown their effects on burning rates of other types of liquid propellants. A 14.9-wt% methanol mixture was examined based on previous studies that showed methanol's effectiveness as a reducing agent in HAN-based propellants. A combination of 14.9 wt% methanol and 1 wt% silica was also studied. The preparation of these formulations is discussed in detail.

Two different methods to measure the burning rates of HAN-based propellants were used in this study. First, a peak-pressure method used the point of highest pressure in the pressure trace to mark the end of the sample combustion. This method has been used successfully with other liquid and solid propellants, but for HAN-based propellants it showed large discrepancies in burning rates when compared to similar formulations

studied by other research groups. An inflection-point method was developed using the results of high-speed video to identify an inflection in the pressure trace as the end of visual burning. This method was applied retroactively to burns that were initially measured with the peak-pressure method.

The peak-pressure method shows an increase in burning rates with the addition of the nanoparticle additives, especially at lower pressures. This method also shows very complex pressure-dependent burning regimes for mixtures containing methanol. The baseline solution with only added methanol increased burning rates at low pressures and a plateau of increased burning rates between 11 and 19 MPa. On the other hand, the methanol solution with the addition of silica has burning rates more similar to the baseline.

As expected, the inflection-point method produces much higher burning rates compared to the peak-pressure method for HAN-based propellant mixtures. The results are in better agreement with similar formulations studied by other groups, although it is unclear whether the resulting burning rate best represents the entire burning of the HAN-based mixture. The inflection-point method shows almost no effect of nanoparticle additives on the burning rates of the baseline HAN mixture. Also, the inflection-point method produces burning rates for the methanol mixtures that are lower than the baseline across most of the tested pressure range. The methanol mixtures also maintain the pressure-dependent burning regimes found with the peak-pressure method.

ACKNOWLEDGMENTS

I would like to thank my research advisor, Professor Eric Petersen, for all of his support and guidance throughout my time as a graduate researcher. I am very grateful for the opportunity he has given me to perform research and study as a graduate student in his laboratory. I have learned many things and gained many skills in the past two years with his help, and I will never forget the experience. I would also like to thank my other committee members, Professor Tim Jacobs and Professor Adonios Karpetis, for their support and instruction both in my research and coursework.

I would like to thank all of my professors at Texas A&M University during my undergraduate and graduate studies for fostering my love of science and engineering. The knowledge and wisdom I have gained from all of my instructors is invaluable to me and continues to shape me to be a better engineer and person. Also, I want to thank all of my fellow researchers in the Petersen Research Group. I will never forget their support and friendship that helped make my time in the lab successful and rewarding.

A special thanks to my good friends Adam Johnson, Justin Ruiz, Arturo Mateos, Matthew Stepter, and Joseph Stocks. Thanks to Katherine Collette for putting up with me through all of this and for always being encouraging.

Finally, I would like to thank my family. Penny, the dog, for “staying up” with me through long nights of studying. My brother and sister for being incredible role models and friends. Most of all, I thank my mother and father for their endless inspiration, support, and love.

NOMENCLATURE

Symbols

d_i	Burner tube inner diameter
d_o	Burner tube outer diameter
$d_{o,pix}$	Burner tube outer diameter measured in pixels
m	Burned propellant mass
P	Chamber pressure
r_b	Burning rate
Y_i	Individual propellant component mass fraction
Δr_b	Change in burning rate
Δt	Total burning time
Δx	Burned propellant axial length
Δx_{pix}	Burned propellant axial length measured in pixels
ρ	Overall propellant mixture density
ρ_i	Individual propellant component density
wt%	Percentage by weight

Common Acronyms

AN	Ammonium nitrate
EIL	Energetic ionic liquid
HAN	Hydroxylammonium nitrate

LGP	Liquid gun propellant
LP	Liquid propellant
MMH	Monomethylhydrazine
PFV	Photron FASTCAM Viewer
ProPEP	Propellant Performance Evaluation Program
TEM	Transmission electron microscopy
TEAN	Triethanolammonium nitrate
UDMH	Unsymmetrical dimethylhydrazine

TABLE OF CONTENTS

	Page
ABSTRACT	ii
ACKNOWLEDGMENTS.....	iv
NOMENCLATURE.....	v
TABLE OF CONTENTS	vii
LIST OF FIGURES.....	ix
LIST OF TABLES	xi
1. INTRODUCTION.....	1
1.1 Motivation for Current Study.....	1
1.2 Overview of Thesis	2
2. BACKGROUND.....	4
2.1 Hydroxylammonium Nitrate (HAN).....	4
2.2 Previous Studies	5
3. EXPERIMENTAL METHODS.....	12
3.1 Strand Burner System Overview.....	12
3.2 Chamber Pressures, Light Intensity, and High-speed Video	14
3.3 Burning Times.....	15
3.4 Burning Rates.....	17
3.5 Propellant Sample Preparation and Analysis	18
3.6 Measurement Uncertainty	22
4. RESULTS AND DISCUSSION	24
4.1 82.4% HAN Baseline	24
4.2 Initial Tests of HAN Mixtures with Nanoparticles and Methanol	26
4.3 Re-measured Burning Rates of HAN Mixtures	30
5. CONCLUSIONS.....	34
5.1 Current Study	34
5.2 Future Studies.....	37

REFERENCES	39
APPENDIX A	45
APPENDIX B	46

LIST OF FIGURES

	Page
Figure 1. Burning rates of aqueous HAN solutions studied by Katsumi et al. [8].	8
Figure 2. Burning rate measurements of a baseline 82.4 wt% HAN solution from McCown and Petersen [8, 34] compared with HAN solutions from Katsumi et al. [8].	10
Figure 3. Burning rate measurement of aqueous HAN solutions containing methanol from McCown and Petersen [20, 34] compared with similar solutions from Chang et al. [20].	10
Figure 4. Custom propellant mount used to house and ignite liquid-based monopropellants in the strand burner.	13
Figure 5. Typical pressure trace of a HAN-based propellant burn with peak-pressure and inflection-point definitions of burning time shown.	16
Figure 6. TEM images of nano-scale particle additives: a) fumed silica and b) titania [32].	20
Figure 7. Burning rates of baseline 82.4% HAN measured with inflection-point method compared with peak-pressure method by McCown and Petersen [34] and a similar formulation measured visually by Katsumi et al. [8].	24
Figure 8. Burning rates of individual batches of baseline 82.4% HAN compared with an 82.5% HAN formulation by Katsumi et al. [8].	25
Figure 9. Burning rates of baseline HAN and baseline with 1% and 3% silica additives [35].	27
Figure 10. Burning rates of baseline HAN and baseline with 1% and 3% titania additives [35].	28
Figure 11. Burning rates of baseline HAN and baseline with 14.9% methanol and 14.9% methanol/1% silica additives [35].	29
Figure 12. Burning rates of re-measured baseline HAN and baseline with 1% and 3% silica additives.	30

Figure 13.	Burning rates of re-measured baseline HAN and baseline with 1% and 3% titania additives.	31
Figure 14.	Burning rates of re-measured baseline HAN, baseline with 14.9% methanol and 14.9% methanol/1% silica, and HAN269MEO15 [20].	32
Figure 15.	Density measurement results from the current study compared to the regression developed by Sassé et al. [21] and the results reported by Vosen [7].	45

LIST OF TABLES

		Page
Table 1.	Selected physical and performance characteristics for HAN269MEO15, an aqueous HAN and methanol propellant, and hydrazine.	5
Table 2.	Compositions of some HAN-based propellants studied in literature [6, 15].	6
Table B1.	Average chamber pressures and linear burning rates for aqueous 82.4 wt% HAN baseline using peak-pressure method [34] and re-measured with the inflection point method.	46
Table B2.	Average chamber pressures and linear burning rates for HAN baseline with 1 wt% silica additive using peak-pressure method and re-measured with the inflection point method.	47
Table B3.	Average chamber pressures and linear burning rates for baseline HAN with 3 wt% silica additive using peak-pressure method and re-measured with the inflection point method.	48
Table B4.	Average chamber pressures and linear burning rates for baseline HAN with 1 wt% titania additive using peak-pressure method and re-measured with the inflection point method.	48
Table B5.	Average chamber pressures and linear burning rates for baseline HAN with 3 wt% titania additive using peak-pressure method and re-measured with the inflection point method.	49
Table B6.	Average chamber pressures and linear burning rates for baseline HAN with 14.9 wt% methanol using peak-pressure method and re-measured with the inflection point method.	50
Table B7.	Average chamber pressures and linear burning rates for baseline HAN with 14.9 wt% methanol and 1 wt% silica additive using peak-pressure method and re-measured with the inflection point method.	51

1. INTRODUCTION

1.1 Motivation for Current Study

In the field of liquid monopropellants, much interest has been shown in aqueous solutions of hydroxylammonium nitrate (HAN, NH_3OHNO_3) as a potential replacement for hydrazine (N_2H_4). Hydrazine and its organic compounds, monomethylhydrazine (MMH) and unsymmetrical dimethylhydrazine (UDMH), are very common liquid rocket propellants that have been proven reliable over many decades of use. Hydrazine is spontaneously ignitable with nitrogen tetroxide with short ignition delay times. As a monopropellant, hydrazine can be decomposed by several suitable catalyst materials. This catalytic decomposition is well understood and has been used for gas generator and attitude control thruster applications [1, 2].

Although hydrazine is established and widely used, it is also highly toxic and carcinogenic [1]. During propellant loadings, many precautions are necessary, including self-contained atmospheric protection ensemble (SCAPE) for workers, constant air quality monitoring, and worker health monitoring. The costs and hazards associated with the handling of hydrazine have led to the pursuit of alternative propellants. Energetic ionic liquids (EILs), peroxides, and others have been considered as possible “green” propellant replacements [3]. Propellant solutions containing HAN, which is an EIL, are promising because they offer a much lower toxicity and higher specific impulse when compared with hydrazine [2, 4].

Pure hydroxylammonium nitrate is a hygroscopic solid that is a potential solid propellant or, when in aqueous solution, a liquid monopropellant. HAN-based liquid propellants are typically composed of three major ingredients: HAN, water, and a reducing agent, such as triethanolammonium nitrate (TEAN) or methanol. The physical properties (e.g. viscosity) and combustion characteristics (e.g. burning rate) of HAN-based propellants can be greatly altered based on percent water and reducing agent content, as well as the inclusion of nanoparticle additives [5-9].

While HAN-based propellants are the front-runners as suitable hydrazine replacements, there are still some challenges hindering their acceptance. For instance, work is on-going to find an effective ignition method [10-12]. The storability of HAN mixtures is also in question, as HAN is known to slowly decompose even with fairly compatible materials [1, 13]. Finally, HAN-based propellants can exhibit combustion instabilities, as well as very high burning rates and flame temperatures compared to hydrazine [6, 9, 11, 14-17]. A better understanding of these phenomena is critical to the development of HAN-based propellants as alternatives to hydrazine.

1.2 Overview of Thesis

The goal of this thesis is to expand upon the research community's understanding of the combustion of aqueous solutions of hydroxylammonium nitrate with and without nanoparticle additives and methanol. This thesis will also detail several experimental techniques that have been developed to better characterize HAN-based propellant

mixtures. Burning rates are presented from two different methods that provide new perspective to the burning behavior of HAN-based propellant mixtures.

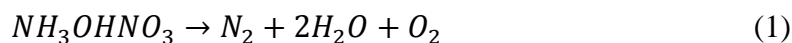
First, background information on HAN, its properties, and combustion, as well as relevant studies will be provided. The next section discusses the experimental techniques used by the author to prepare propellant samples and to study their burning behavior. Included in the techniques section are descriptions of the instrumentation and detailed error analysis. Results from composition studies are discussed in order to address the possibility of bad formulations of the HAN solutions. Next, burning rate measurements are presented from two distinct methods; a peak-pressure method and an inflection-point method are each used to identify the end of the burning. Finally, the agreement of these two methods and comparison with results from other groups will be discussed.

The experimental techniques described in this thesis aim to close a gap in the understanding of HAN-based propellant combustion. However, the use of two different methods of measuring burning rates has also led to more questions about the propellant's burning behavior. A significant pressure rise after the end of visible burning requires more study to understand if there are more chemical reactions occurring that are not accounted for.

2. BACKGROUND

2.1 Hydroxylammonium Nitrate (HAN)

Hydroxylammonium nitrate (HAN), with chemical formula NH_3OHNO_3 , is an inorganic nitrate salt. HAN is a hygroscopic opaque solid at room temperature and has a melting temperature of 48°C [18]. Aqueous HAN is an energetic ionic liquid consisting of cation NH_3OH^+ and anion NO_3^- in water. Reactions of HAN show oxidation of NH_3OH^+ and reduction of NO_3^- , making HAN a monopropellant [19]. The global decomposition reaction of HAN is shown in Equation (1).



The excess oxygen in the reaction shown in Equation (1) indicates more energy could be released by the inclusion of another fuel. Therefore, many HAN-based propellants include organic reducing agents, such as methanol or TEAN. The properties of propellants consisting of HAN, water, and fuel can be adjusted based on the relative amounts of each ingredient. This tunable nature of HAN-based propellants has made them strong candidates for replacing hydrazine. One such propellant is HAN269MEO15, a mixture of HAN, ammonium nitrate (AN), methanol, and water [20]. Table 1 shows a comparison of the physical and combustion performance of HAN269MEO15 with hydrazine. The values in the table were calculated using Propellant Performance Evaluation Program (ProPEP). HAN269MEO15 and other HAN-based propellants are discussed in more detail in the next section.

Table 1. Selected physical and performance characteristics for HAN269MEO15, an aqueous HAN and methanol propellant, and hydrazine.

Propellant	HAN269MEO15	Hydrazine
Molecular Weight (g/mol)	49.07	32.05
Density (g/cm ³)	1.360	1.013
Specific Impulse (s)	266.3	233.8
Density Impulse (g-s/cm ³)	362.2	236.8
Adiabatic Flame Temperature (°C)	2182	1121
LD ₅₀ Toxicity (mg/kg)	325	60

2.2 Previous Studies

HAN-based propellants were first extensively studied by the U.S. Army for liquid gun propellant (LGP) applications. The incentives for LGPs were the caseless ammunition, increase in muzzle velocity, and improved logistics, as proposed by personnel at Naval Ordnance Station, Indian Head, MD [19]. Studies included chemical and physical property analysis [5, 21, 22], material compatibility [13], and combustion [6, 7, 16, 17, 23] of mixtures of HAN and TEAN in water. The two liquid propellants (LPs) of interest were LP 1845 and LP 1846. The combustion of these propellants along with several aqueous HAN mixtures of varying water content was studied using strand burners [6, 7, 16, 17, 23, 24] and atomization sprays [25, 26] over a range of pressures from atmospheric to 200 MPa. Table 2 shows a number of HAN-based propellant mixtures from the literature. Percentages by weight (wt%) are used to quantify constituent concentrations.

Table 2. Compositions of some HAN-based propellants studied in literature [6, 15].

Propellant Name	HAN	Water	Fuel	AN
LP 1845	63.2 wt%	16.8 wt%	TEAN 20.0 wt%	N/A
LP 1846	60.8 wt%	20.0 wt%	TEAN 19.2 wt%	N/A
XM46	60.8 wt%	20.0 wt%	TEAN 19.2 wt%	N/A
HANGLY26	60.0 wt%	26.0 wt%	Glycine 14.0 wt%	N/A
HAN269MEO15	69.7 wt%	14.91 wt%	Methanol 14.79 wt%	0.60 wt%
HAN284MEO17	77.25 wt%	4.89 wt%	Methanol 17.19 wt%	0.67 wt%

Vosen showed that HAN mixtures had different regimes of burning behavior over different pressure ranges [6, 7, 23]. Furthermore, difficulties were discovered in the determination of the burning rates of HAN propellants because of surface instabilities. The instabilities were thought to increase the apparent burning rates by increasing the burning surface area [16, 23, 24]. Gelled versions of the propellants were also studied [16, 17]. For gelled propellants, the burning surface was observed to be flat, which was attributed to increased surface stability due to the higher viscosity. Vosen proposed that the combustion of HAN-based propellants was staged: first, condensed-phase decomposition of HAN occurs, then gas-phase reaction of HAN products and TEAN [6].

Chang et al. [15, 20] and Katsumi et al. [8, 14] studied HAN-based propellants with glycine or methanol as reducing agents and small percentages of AN. The burning

rates of these propellants were measured using visual techniques at pressures between 0.7 and 15 MPa. Like Vosen [23], Chang et al. [15] found pressure-dependent regions in the flame structure of XM46, a propellant equivalent to LP 1846. Both Vosen and Chang et al. found that the flame could be divide into 3 regions in order from the burning surface: 1) dark opaque gases, 2) transparent gases, and 3) luminous flame. A luminous flame was only observed at pressures higher than 28 MPa, and as pressure decreased the opaque layer grew in thickness until the transparent layer could no longer be seen below a pressure of 13 MPa.

Due to the relative complexity of HAN mixtures, combustion mechanisms have not yet been understood fully. Van Dijk and Priest studied the decomposition of an 11 molar HAN solution using Raman spectroscopy over a pressure range of 200 to 700 MPa and temperature range of 22 to 120°C [27]. Using deflagration theory and asymptotic analysis, Shaw and Williams found that condensed-phase reactions control HAN deflagration rates [28]. The researchers supported postulates that HAN decomposition was controlled by the rate of proton transfer from NH_3OH^+ to NO_3^- [27] and that phase and chemical equilibrium are not reached in the HAN decomposition zone. Lee and Litzinger chose eight reactions as a reduced reaction model for HAN decomposition that simulated experimental data well [29].

Katsumi et al., recognizing the difficulties of modeling complex mixtures of HAN, studied numerous aqueous HAN solutions of differing HAN weight percentages without additives [8]. In the study, burning rates were measured using high-speed video at pressures between 0.5 and 10 MPa. The burning rate data for some high HAN-content

solutions were compared to results from crystalline HAN [9] as shown in Figure 1. Katsumi found that the combustion behavior of the solutions over that pressure range could be categorized based on the appearance of bubble formation at the combustion surface. The combustion wave structure was proposed to fall in one of two categories: 1) at low burning rates, the water completely vaporizes in a thin, two-phase region after which the reaction zone takes place; and 2) at high burning rates, the two-phase region is much longer and the majority of the reaction takes place within bubbles in that zone. Furthermore, Katsumi proposed that superheat, the difference between the temperature in the gas-phase bubbles and the water boiling temperature, could cause a very high vapor nucleation rate. In turn the burning rate of the solution could appear very high due to rapid vapor nucleation.

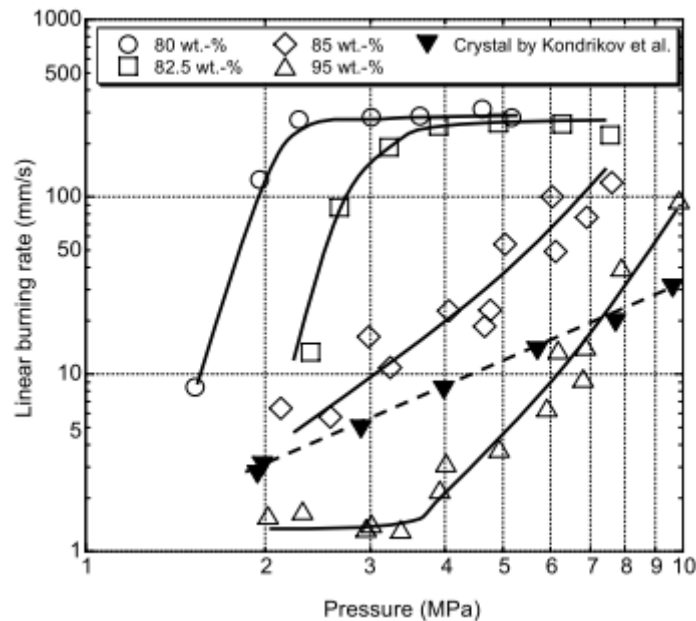


Figure 1. Burning rates of aqueous HAN solutions studied by Katsumi et al. [8].

The addition of particle additives has been shown to significantly alter the combustion behavior of liquid monopropellants and increase burning rates. Some of these studies have included synthesized alumina catalysts dissolved in JP-10 [30], aluminum powder mixed with water [31], and three-part mixtures of aluminum, water, and hydrogen peroxide [3]. McCown and Petersen studied the effects of aluminum, silica, and titania nanoparticle additives on the combustion of nitromethane using a pressure-based method of measuring burning rates [32, 33]. The results of that study also showed good agreement between their pressure-based method and traditional visual methods.

As stated before, early studies of HAN-based propellants sometimes used gelling additives. McBratney et al. used xanthan and rhamsan gum to stabilize the burning of XM46 [16, 17]. The study of nanoparticles additives on HAN-based propellants is a very new field. The effects of silica and titania nanoparticles on the burning rates of aqueous solutions of HAN or HAN and methanol have been studied using a pressure-based method [34, 35]. These studies found the pressure-based method for aqueous HAN mixtures produced much slower burning rates compared to other groups using visual methods. Figure 2 shows the results of McCown and Petersen [34] compared with Katsumi et al. [8] for burning rates of aqueous HAN solutions. Figure 3 shows the results of McCown and Petersen [34] compared with Chang et al. [20] for the burning rates of aqueous HAN mixtures containing methanol.

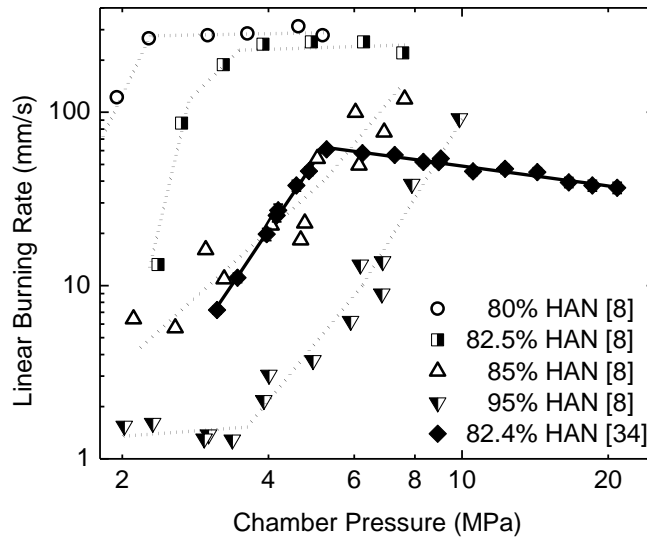


Figure 2. Burning rate measurements of a baseline 82.4 wt% HAN solution from McCown and Petersen [8, 34] compared with HAN solutions from Katsumi et al. [8].

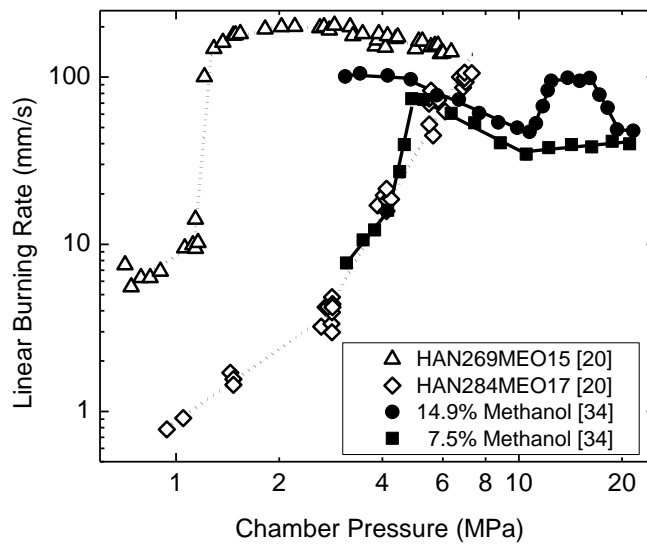


Figure 3. Burning rate measurement of aqueous HAN solutions containing methanol from McCown and Petersen [20, 34] compared with similar solutions from Chang et al. [20].

Stahl et al. sought to address this discrepancy by measuring the burning rates of nitromethane or aqueous HAN samples with both pressure- and visual-based methods simultaneously [36]. For aqueous HAN, Stahl et al. discovered that chamber pressures continued to rise significantly after the sample visually appears to be done burning. They suggested that there were reactions still occurring but not visible on the camera. This observation may be in agreement with Katsumi's proposition that a high vapor nucleation rate could make HAN burning rates appear high [8] and with Shaw and Williams' proposition that chemical and phase equilibrium does not occur in the HAN reaction zone [28].

3. EXPERIMENTAL METHODS

3.1 Strand Burner System Overview

The strand burner used in this study consists of a cylindrical test chamber with an inner diameter of 94 mm (3.70 in.), a height of 203 mm (8.00 in.), and two optical ports surrounding the propellant sample holder. Pressurized gas is fed through a line that connects to a port on the side of the chamber. The chamber is exhausted through a port on the top. A large threaded hole centered on the bottom surface is used to insert a propellant sample holder that resembles a large bolt. The holder also contains electrodes used for the ignition of the propellant samples. This system has the ability to record the instantaneous pressure, light intensity, and high-speed video of a small sample of solid or liquid propellant throughout the combustion process. A picture of a HAN sample in the strand burner before ignition is shown in Figure 4.



Figure 4. Custom propellant mount used to house and ignite liquid-based monopropellants in the strand burner.

The strand burner is separated from a control room by reinforced concrete walls, a 1.5-in. blast door, and an additional fire door. From the control room, the pressure of the strand burner can be controlled by two solenoid valves, one for pressurizing and one for venting. During testing operations, the test cell remains empty until the strand burner has been completely vented and depressurized. Additional details regarding the strand burner hardware and attached pressurization systems may be found in the thesis by Warren [37].

A segment of fused quartz tubing was inserted into the central mount cavity to hold the propellant samples. The segment had an outer diameter of 9 mm and an inner

diameter of 7 mm, holding approximately 1.0 g of propellant. The tube was also sealed with Teflon tape on one end to prevent liquid from escaping out of the bottom.

A 30-gauge nickel-chromium wire was placed in contact with the surface of the sample and connected between the two electrodes. The ignition circuit was completed via a Struthers-Dunn 0339AF electric relay connecting the propellant mount electrodes to a GW Instek SPS-3610 power supply. To ignite the propellant, the relay was energized, allowing a current of 6 A to pass through the wire to heat it above 1000 °C and ignite the propellant sample. This relay remained energized throughout the duration of the test, and the circuit was broken soon after ignition by the disintegration nickel-chromium wire.

The strand burner was pressurized to the desired conditions using compressed argon, enabling the authors to measure the combustion behavior of HAN mixtures over a wide range of ambient pressures. As the strand-burner was filled from the control room, the pressure was monitored on a digital gauge. Once the desired pressure was indicated by the gauge, the fill valve was close and the test could proceed. The use of argon also ensured the propellant sample burned as a monopropellant without the addition of a gaseous oxidizers or other reactants.

3.2 Chamber Pressures, Light Intensity, and High-speed Video

The strand burner's instantaneous pressure is measured by an OmegaDyne PX02C1-7.5KG5T pressure transducer at a rate of 1 kHz. The intensity of light emitted by a burning propellant sample was measured using a New Focus 2031 silicon

photodiode detector. Both the pressure transducer and the photodiode were connected to a computer in the control room, which used GageScope software to record their data via a computer-mounted oscilloscope board from Gage. The oscilloscope was manually triggered just before the ignition of the propellant, and the pressure and light intensity data were saved to ASCII-formatted files immediately after the completion of the burn. The resulting data files were imported into Origin 8.07 software for conversion from voltage to the appropriate units and post-processing.

In addition to pressure and light intensity data, high-speed video could be recorded for some propellant burns. A Photron FASTCAM SA3 high-speed camera was used to take video of baseline HAN mixtures at 250 fps. The relatively low frame rate was necessary to view the propellant sample burning surface because HAN flames did not give off any visible light. Furthermore, an LED was used to illuminate the propellant sample inside the strand-burner. The video camera was remotely triggered from the control room using Photron FASTCAM Viewer (PFV) software. The PFV software was also used to take measurements of burning times and distance and save compressed video files. For more details of the video system used, see the study by Stahl et al. [36].

3.3 Burning Times

A typical HAN-based propellant pressure trace during a burn is shown in Figure 5. Overlaid on the plot are markers made to identify key points during the burn. The first black cross at the beginning of the pressure rise identifies the start-time and -pressure of the burn, defined as the intersection of a horizontal line created by the initial pressure

and a sloped line created by the initial pressure rise. The grey cross marks the end-time and -pressure of burn when defined as the point of highest pressure. The peak-pressure definition was used by McCown and Petersen for nitromethane [32, 33] and early HAN-based propellant studies [34, 35]. The second black cross, usually found around 75% of the total pressure rise, identifies the end-time and -pressure of the burn when defined as an inflection point in the pressure trace after which the pressure rises more slowly and in an irregular manner. The inflection-point definition for the end time was identified by Stahl et al. by comparing pressure trace data and high-speed video [36]. Stahl et al. found that the inflection point in the pressure trace consistently corresponded to the point in time when the burning surface of the sample reached the bottom of the quartz tube. The new definition for the end-time and -pressure of burning can be applied retroactively to allow to data taken without high-speed video.

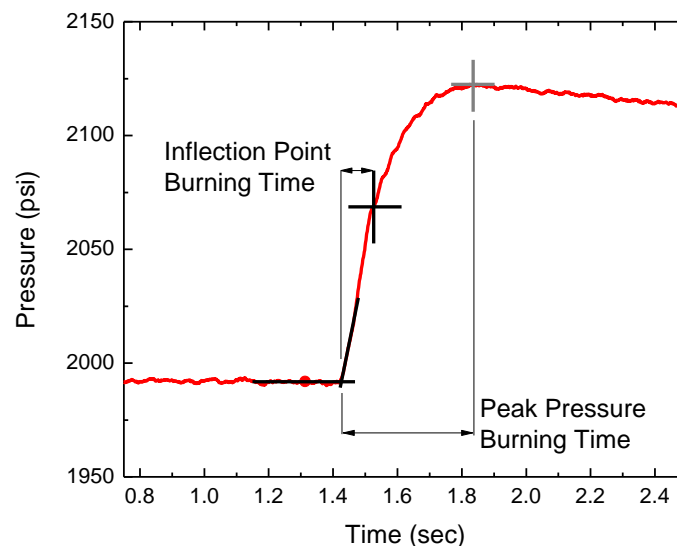


Figure 5. Typical pressure trace of a HAN-based propellant burn with peak-pressure and inflection-point definitions of burning time shown.

For either definition used to identify the burn end-time, the test pressure and burn-time are calculated the same way, but produce different burning rate results. The test pressure is defined as the average of the initial and final pressures. The definition of the end-time has very little effect on the calculated test pressure, because the pressure rise during a burn is very small compared to the overall pressure in the strand burner. On the other hand, the total burn-time is defined as the difference between the end-time and start-time, and the definition of end-time does significantly alter this value.

3.4 Burning Rates

A propellant sample's average burning rate was calculated by knowing the distance (Δx) and time (Δt) over which the burning surface regressed in the quartz tube. For video-based burning rate measurements, all that was needed was a known reference length in the video to serve as a conversion from pixel distance to millimeter distance. The conversion factor was attained from the known outer diameter of the quartz tube (d_o) and its measured diameter in pixels ($d_{o,pix}$). Combining these terms leads to an equation for the burning rate given by Equation (2)

$$r_b = \frac{\Delta x}{\Delta t} = \frac{\Delta x_{pix} * \left(\frac{d_o}{d_{o,pix}} \right)}{\Delta t} \quad (2)$$

For pressure-based burning rate measurements, the total propellant sample height was used as the burn distance. The height of the propellant sample was calculated from the measured initial propellant mass (m), the known quartz tube inner diameter (d_i), and

the calculated density of the propellant mixture (ρ). Combining these terms leads to another equation for the burning rate given by Equation (3).

$$r_b = \frac{\Delta x}{\Delta t} = \frac{4m/(\pi\rho d^2)}{\Delta t} \quad (3)$$

The mass of the propellant sample was measured by placing the entire sample mount on an Ohaus ARA520 digital scale and adding propellant with a pipette until the surface was a reasonable distance from the top of the quartz tube. The sample's mass was then simply the mass added during this process. The diameter of the quartz tube was provided by the manufacturer and also verified using a caliper. The propellant mixture density was calculated from the densities of its constituents. This calculation is detailed in the next section.

3.5 Propellant Sample Preparation and Analysis

The burning characteristics of HAN-based propellants have been shown to be very sensitive to composition [8]. Furthermore, pressure-based burning rate measurements depend on the propellant density, which is a function of the concentrations of the various mixture constituents. It was therefore very important in this study to have an accurate understanding of the propellant mixture compositions and densities before conclusions could be drawn from burning data.

Aqueous HAN solution was purchased from Sigma-Aldrich Co. at 24 wt% HAN. To increase the concentration to 82.4 wt% HAN, the original solution was evaporated in a vacuum chamber for several days. By measuring the mass of water lost, the new

weight percentage of HAN could be determined. As long as the new weight percentage was greater than the targeted 82.4%, dilute HAN could be added at the appropriate amount to achieve that concentration.

Methanol was chosen as a reducing agent due its proven compatibility in past aqueous HAN/methanol studies by Chang et al. [20] and Katsumi et al. [14]. The anhydrous methanol was purchased from Sigma-Aldrich Co. Fumed silica (SiO_2) powder consisting of 200- to 300-nm aggregate particle chains with an average specific surface area of $200 \text{ m}^2/\text{g}$ was purchased from Sigma-Aldrich Co. Titania (TiO_2) particles with a mean diameter of 20 nm and an average specific surface area of $148 \text{ m}^2/\text{g}$ were purchased from Mach I, Inc. These additives were chosen based on previous studies that demonstrated their ability to alter the burning rates of liquid monopropellants [3, 32-34]. Transmission Electron Microscopy (TEM) images of each powder are provided in Figure 6 [32].

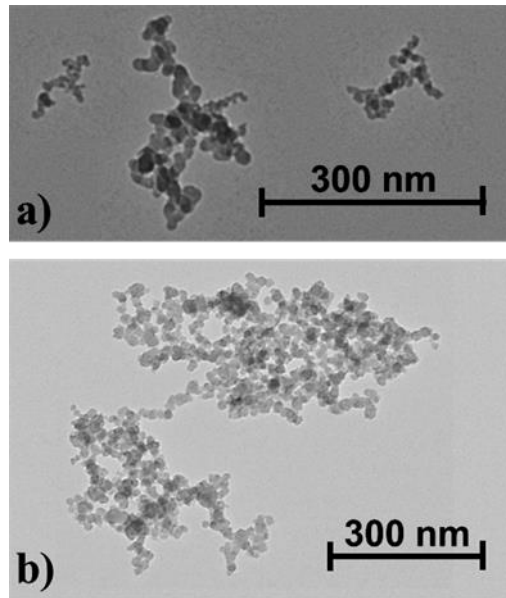


Figure 6. TEM images of nano-scale particle additives: a) fumed silica and b) titania [32].

Propellant mixtures containing nanoparticles were created by placing a beaker of the aqueous HAN solvent on the Ohaus ARA520 scale and adding the desired mass of the additive. Once the appropriate mass was present, the mixture was stirred for several minutes by hand and then placed in a 42-kHz ultrasonic mixer for up to an hour. A particle settling study performed by McCown and Petersen showed that this procedure could stably suspend nanoparticles in aqueous HAN solutions [34]. Nano-sized silica and titania particles were shown to act as effective gelling agents due to their high specific surface areas. However, the study also showed a tendency of these nanoparticles to form large agglomerates. Therefore, in this study the 42-kHz ultrasonic mixer was used to break apart agglomerates and discourage their formation for approximately 30 minutes before each propellant burning test.

The densities of the propellant mixtures were calculated using the known weight fractions (Y_i) and the densities (ρ_i) of each propellant mixture component. Equation (4) provides an example of this calculation for a mixture of HAN, water, silica, titania, and methanol as used in the current study.

$$\rho = \frac{1}{(Y_{HAN/H_2O}/\rho_{HAN/H_2O})+(Y_{SiO_2}/\rho_{SiO_2})+(Y_{TiO_2}/\rho_{TiO_2})+(Y_{CH_3OH}/\rho_{CH_3OH})} \quad (4)$$

This method was numerically equivalent to using the volumetric fractions of the propellant liquid and added particles to calculate the overall density. The densities of the nanoparticle and methanol additives were provided by the suppliers, and could be used in Equation (4) directly. However, aqueous HAN was purchased at a concentration of 24 wt% HAN for which the density was provided as 1.118 g/ml. Because HAN is hygroscopic, the density of aqueous HAN solutions is not linear with concentration (i.e. the density is not equal to the weighted average of the density of crystalline HAN and the density of pure water) [21]. To account for this property, Sasse developed a second-order least squares fit of density measurements obtained from solutions formulated from crystalline HAN using a temperature controlled, U-tube oscillator density meter [21]. The second-degree polynomial written in terms of weight percentages is given as Equation (5).

$$\rho_{HAN/H_2O} = 1.00083 + 4.5813 \times 10^{-3}(\text{wt\% HAN}) + 2.4609 \times 10^{-5}(\text{wt\% HAN})^2 \quad (5)$$

Using Equation (5) for 82.4 wt% HAN yields a density of 1.545 g/ml, which can then be used in Equation (4) to calculate the densities of the other mixtures. Equation (5) also provides a way of evaluating the evaporation process described earlier to create the

concentrated HAN solutions. Density measurements of HAN solutions were made using a Fisherbrand Finnpipette II volumetric pipette and the Ohaus ARA520 digital scale. The results of this study are shown in Appendix A.

HAN has been seen to decompose slowly in storage [13, 18], which further necessitates methods of determining the quality of propellants. Nitric acid (HNO_3) is a key chemical used in the synthesis of HAN and is also used as a stabilizer of HAN solutions [22]. Previous studies examined the presence of excess nitric acid using acid-base titrations with sodium hydroxide (NaOH) [5, 13, 22]. In the current study, attempts were made to detect excess nitric acid using a similar method, but results were inconclusive.

3.6 Measurement Uncertainty

The primary source of uncertainty in the burning rate measurements made in this study stemmed from uncertainty in the measurement of burning time. As stated previously, the start- and end-times for a particular burn were selected based on features in the pressure plot. While these features are present in every plot, inherent signal noise introduce a considerable amount of random error. McCown and Petersen quantified burning time uncertainties based on the upper and lower limits of points that could be reasonable selected as the start and end points in the burn [34]. They then developed an empirical relation between the burning rate and the burning time uncertainty. However, the equation produced results in negative uncertainty values for the high burning rates measured in this study. Furthermore, their analysis only considered the uncertainty in

selecting the start point in the pressure trace and assumed the uncertainty in selecting end point was equal; a liberal assumption given how the sharp initial pressure rise compares to the broad pressure peak at the end of a typical HAN-based propellant burn.

To determine the accuracy for the current study, a new uncertainty analysis was needed. Kline-McClintock uncertainty analysis was performed on Equation (3) with the assumption that the burner tube area was precisely known. A simple sensitivity analysis shows that the uncertainty that would be introduced by including the area is very small compared to the other measurement uncertainties. The uncertainty used for the mass measurement was based on the Ohaus scale resolution error given as ± 0.005 g. The uncertainty of the density was taken from the density analysis discussed before and given as ± 0.01 g/cm³. The uncertainty of the burn time measurement is chosen as ± 0.01 s. Although the true uncertainty in the burn time measurement varied for each trial, this value is a good representation for typical burns.

4. RESULTS AND DISCUSSION*

4.1 82.4%² HAN Baseline

A baseline solution of 82.4% HAN was first tested with the new method of measuring the burning rates. In addition to retro-actively examining data from a previous study by McCown and Petersen [34], two new batches of propellant were prepared and burned. Figure 7 shows the newly determined burning rates compared with the results of an 82.5% HAN solution by Katsumi et al. [8] and the results of McCown [34].

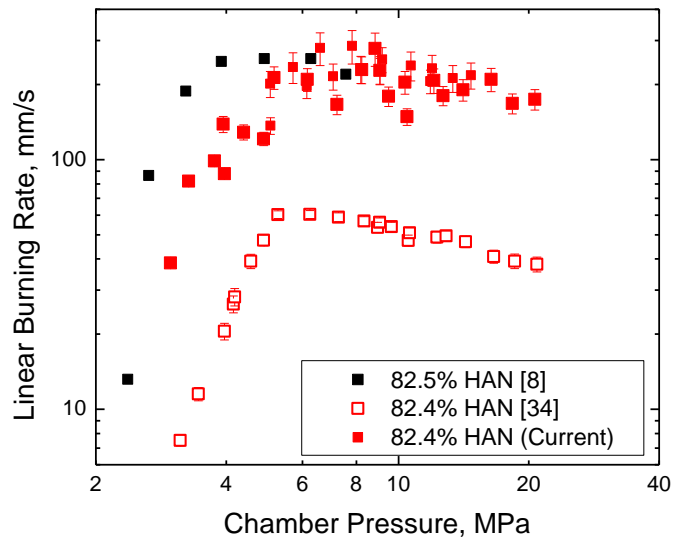


Figure 7. Burning rates of baseline 82.4% HAN measured with inflection-point method compared with peak-pressure method by McCown and Petersen [34] and a similar formulation measured visually by Katsumi et al. [8].

* Part of this section is reprinted from: "Effects of Nano-scale Additives and Methanol on the Linear Burning Rates of Aqueous HAN Solutions," G.D. Homan-Cruz, K.W. McCown, E.L. Petersen, *50th AIAA/ASME/SAE/ASEE Joint Propulsion Conference*, AIAA Paper 2014-3566, Copyright 2014 by G.D. Homan-Cruz, K.W. McCown, E.L. Petersen.

² For the remainder of Section 4, "%" will be used to denote a percentage by weight.

It is seen in Figure 7 that the burning rates produced using the inflection point in the pressure trace as the end point agree with Katsumi's data much more closely. However, the use of this method has brought on a considerable amount of scatter in the data when compared with McCown's results. Whereas McCown was able to produce two linear burning rate equations over the well-defined pressure regimes 3-5 MPa and 5-20 MPa [34], the amount of scatter in the present data prevents such a calculation.

While the present baseline HAN data appear as though they may be less repeatable than Katsumi's data, it is thought that Katsumi's data may only represent a single batch because of the very few number of data points. Figure 8 shows McCown's converted data, and the batches prepared separately for this study compared with each other. The batches are labeled by the date they were created.

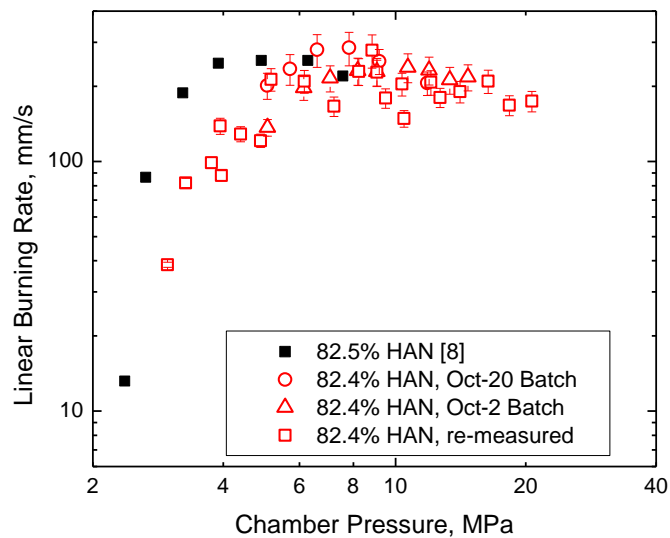


Figure 8. Burning rates of individual batches of baseline 82.4% HAN compared with an 82.5% HAN formulation by Katsumi et al. [8].

The individual batches shown in Figure 8 show similar trends, although they occur at different burning rates and pressures. All data sets show a peak burning rate occurring between 5 and 8 MPa. The error bars included in the graph show the burning rate differences between batches are within the measurement uncertainty. The Oct-2 and Oct-20 batches also represent the only batches in this study that had high-speed video recordings. Their burning rates were verified with the high-speed video, therefore the uncertainty in their burning rates can be considered much smaller than the error bars would indicate.

4.2 Initial Tests of HAN Mixtures with Nanoparticles and Methanol

As with the baseline 82.4% HAN, initial studies of the baseline with additives were done using the peak-pressure definition of the burning end point. As mentioned above, fumed silica powder was selected as a burning rate modifier based on McCown and Petersen's previous study that observed significant combustion improvements in nitromethane from the inclusion of small concentrations of metal oxide additives [32]. The current study examined the effects of increasing the amount of silica to 3.0% from 1.0%, which was also shown to increase the burning rates of HAN-based propellants [34]. Figure 9 shows the burning rate results of baseline HAN compared with aqueous HAN mixtures containing 1% silica or 3% silica.

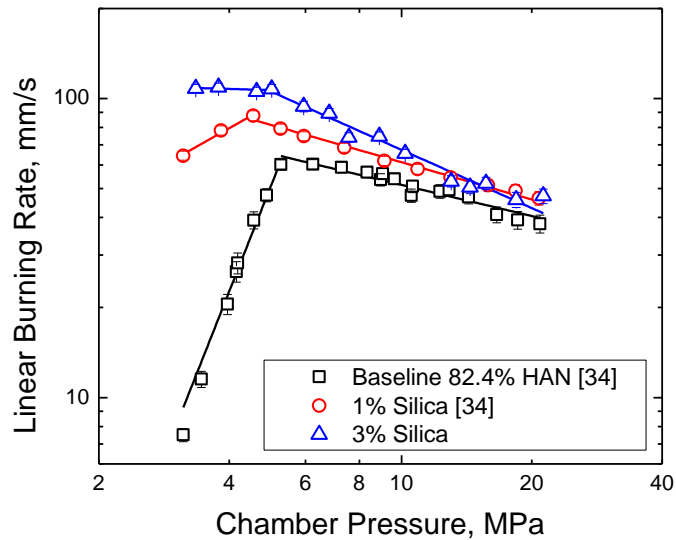


Figure 9. Burning rates of baseline HAN and baseline with 1% and 3% silica additives [35].

The addition of nano-sized silica shows increased burning rates at all pressures tested, although much less significant an increase at pressures above approximately 10 MPa. Also, below 10 MPa, the higher concentration of 3% silica shows slightly higher burning rates than the lower concentration.

Previous work by McCown and Petersen showed that, as with fumed silica, small concentrations of titania could also increase the burning rate of nitromethane [32]. Therefore, titania was chosen for this study to examine its possible effects on the combustion of aqueous HAN mixtures. Figure 10 shows the burning rate results of baseline HAN compared with aqueous HAN mixtures containing 1% titania or 3% titania.

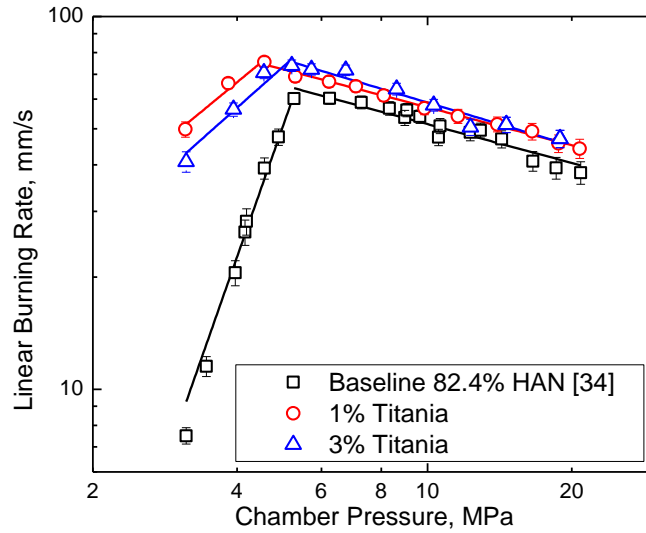


Figure 10. Burning rates of baseline HAN and baseline with 1% and 3% titania additives [35].

The HAN mixtures containing nano-sized titania particles show a similar trend to the mixtures with silica. That is, across all pressures the burning rates are higher for the mixtures with additives when compared with the baseline. Also, as with silica, mixtures containing titania have much higher burning rates at pressures below 5 MPa and little to no effect on burning rates at pressure below this threshold. Contrary to the silica mixture, the 3% titania mixture has lower burning rates than the 1% titania mixture at pressures below 5 MPa. This trend with increasing particle concentration is the opposite of the behavior shown with the 1% and 3% silica mixtures.

The decision to use methanol as a burning rate modifier was motivated by the success of previous studies of HAN/AN/methanol-based propellants and a desire to significantly expand the range of tested pressures for similar mixtures [14, 20].

Furthermore, the combination of methanol with fumed silica was studied because each individually proved to have significant effects on the burning rate magnitude and profile of HAN. Figure 11 shows the burning rate results of baseline HAN compared with aqueous HAN mixtures containing 14.9% methanol or 14.9% methanol and 1% silica.

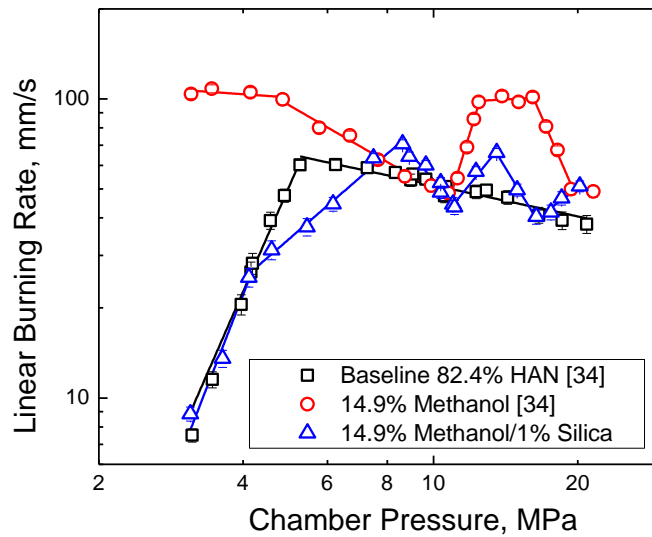


Figure 11. Burning rates of baseline HAN and baseline with 14.9% methanol and 14.9% methanol/1% silica additives [35].

The addition of methanol in HAN mixtures resulted in complex, pressure-dependent burning regimes. The mixture containing 14.9% methanol has much higher burning rates at low pressures and an interesting plateau feature between 10.8 and 19.4 MPa. As with the 14.9% methanol mixture, the mixture containing both 14.9% methanol and 1.0% silica showed a complex burning rate profile. However, the addition of 1.0% silica greatly altered the burning behavior in certain regimes. Primarily, the burning rate was decreased across the entire pressure range, except for a small region between 7.5 and 10.3 MPa where the burning rates were slightly higher. The most drastic change

occurred at pressures below 4.1 MPa, where the mixture's burning rates were very similar to the baseline's. The mixture containing 14.9% methanol and 1.0% silica also showed a peak, rather than a plateau, between 11.1 and 16.4 MPa, with the peak occurring at 13.5 MPa. The burning rate was decreased from the plateau to the peak by 35%.

4.3 Re-measured Burning Rates of HAN Mixtures

With the development of the new method of measuring burning rates using the inflection point in pressure trace as the end point, the data collected in the previous section were re-measured. Figure 12 shows the results of the re-measured burning rates of baseline HAN with nano-sized silica additives compared with the baseline HAN burning rates containing both new and re-measured data with the same technique.

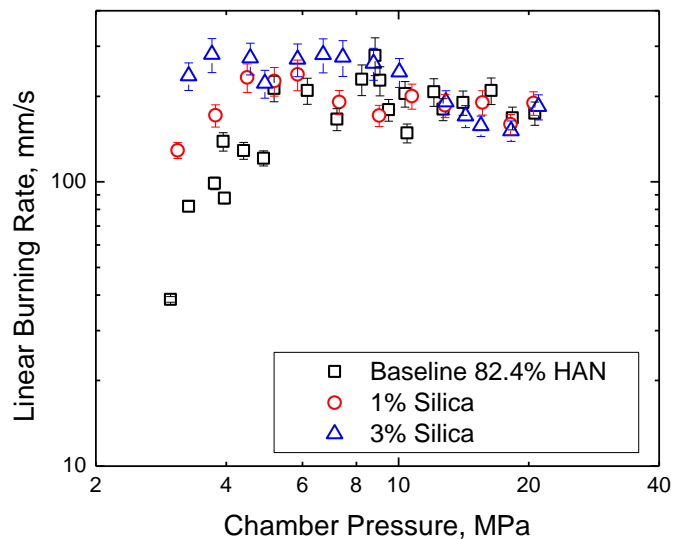


Figure 12. Burning rates of re-measured baseline HAN and baseline with 1% and 3% silica additives.

While the results for silica mixtures appear much less conclusive than with the peak-pressure method, some general trends remain. First, at pressures below 5 MPa the burning rates of mixtures containing silica additives are higher than the baseline. Also, as with the previous method, below 10 MPa the mixture containing 3% silica has higher burning rates than the mixture with only 1% silica. That fact that silica was shown to shorten the burning time when the whole pressure rise was considered and had a much less effect when only the liquid propellant vaporization was considered suggests the silica's contribution to the propellant burning must take place in the mixed or gas phases.

The re-measured burning rates for HAN mixtures containing 1% and 3% titania compared with baseline HAN are shown in Figure 13.

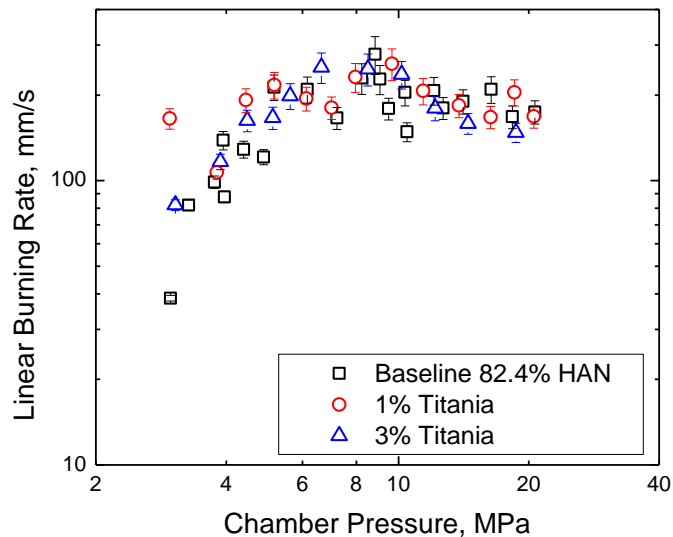


Figure 13. Burning rates of re-measured baseline HAN and baseline with 1% and 3% titania additives.

As with silica, the effect of titania additives is much less apparent with the re-measured burning rates. While at low pressures below 5 MPa the titania may increase

burning rates, the results are inconclusive. Furthermore, at pressures above 11 MPa the added titania appears to decrease the burning rates. Again, the fact that the re-measured burning rates show a much lower sensitivity to particle additives indicates the contribution of these particles lies in the pressure rise (i.e., gas-phase burning) that is not accounted for using the inflection point method.

Finally, the burning rates of mixtures of baseline HAN with 14.9% methanol or 14.9% methanol and 1% silica were re-measured with the inflection-point method. The results of the analysis with the alternative method are shown in Figure 14.

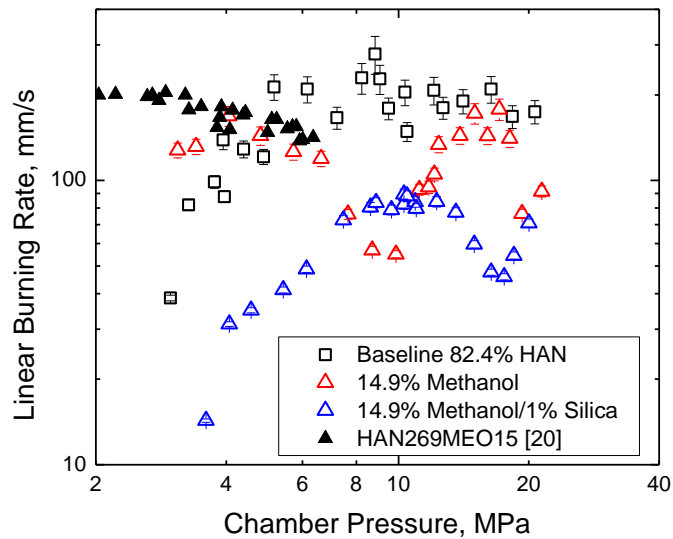


Figure 14. Burning rates of re-measured baseline HAN, baseline with 14.9% methanol and 14.9% methanol/1% silica, and HAN269MEO15 [20].

The burning rates of the mixtures containing methanol did not change as much as other mixtures between the peak-pressure and the inflection-point methods. However, the new method did lead to better agreement between the 14.9% methanol mixture and HAN269MEO15 [20]. The pressure-dependent features found in the burning rates of the

14.9% methanol mixture were essentially the same between the two methods: an initial pressure independent regime at pressures below 7 MPa, a regime of decreasing burning rates between 7 and 10 MPa, a plateau between 11 and 19 MPa at a burning rate similar to the regime below 7 MPa, and finally a decrease in burning rates above 19 MPa. For the 14.9% methanol and 1% silica mixture, the peak burning rate at 13.5 MPa that was seen with the peak-pressure method was instead the end of a plateau with the inflection-point method. For the inflection-point method, the methanol/silica mixture shows significantly lower burning rates compared to the baseline over the entire pressure range. All of the data presented in the preceding sections are provided in Tabulated form in Appendix B.

5. CONCLUSIONS

5.1 Current Study

The study presented by this thesis shows the work that has been done to better understand the combustion of aqueous HAN and its mixtures with other additives. The study has shown results from two separate methods of defining the burning rates of aqueous HAN samples: the peak-pressure burning time method and the inflection point burning time method. While the peak-pressure method was shown to work well with nitromethane propellants [32, 33], it was shown to produce very different burning rates for aqueous HAN mixtures when compared to other groups using visual-based techniques. For this reason, a new method was introduced based on the results from video measurements that identified an inflection point in the burning pressure trace as the end time of visual burning [36]. The inflection point could be identified in nearly all HAN-based propellant pressure traces and could, therefore, be retroactively used to produce new burning rates for burns performed before the method's development in the author's laboratory.

Comparisons were made between the burning rate results of the two methods that showed some similarities and differences. For the baseline aqueous HAN propellant, the burning rates appeared much higher, as expected, with the inflection point method. The results also agree with a similar mixture studied by Katsumi et al. [8]. The cause of the pressure rise after the inflection point is still unknown, but is thought to be the product of later, secondary reactions in the gas phase. If this second-stage burning is the case, the

apparent burning rates produced by the visually observed regression of the burning surface may be better described as the measure of the vaporization rate in agreement with Katsumi et al. [8].

In general for the mixtures containing nanoparticle additives without methanol, the burning rates were seen to be increased significantly compared to the baseline for the peak-pressure method. However, the burning rates were not conclusively different between the nanoparticle mixtures and the baseline for the inflection point method. This would indicate that the additives accelerate the burning in the time after the inflection point. While it was previously thought that the use of gelling agents could decrease the burning rates of HAN-based propellants by providing a more stable burning surface [16, 17], there was also evidence to show the particular additives used in this study could increase the burning rates by aiding vapor nucleation and having catalytic effects on nitromethane [32]. It may be that these opposing effects cancel each other. However, the fact that burning rates taken using the peak-pressure method show increased burning rates with the nanoparticles indicates there is an effect of the additives during the pressure rise after the inflection point.

Mixtures containing methanol showed complex, pressure-dependent burning behavior for burning rates measured with both peak-pressure and inflection point methods. The burning rates were not increased as significantly by applying the inflection-point method for the methanol-containing mixtures as they were for the nanoparticle mixtures. However, the 14.9% methanol mixture results from the inflection point method were in better agreement with the similar mixture, HAN269MEO15.

The pressure-dependent features found in the burning rates of the 14.9% methanol mixture are nearly the same between the two methods. The major difference observed between the two methods lies in the relative change in burning rates from the baseline. For the inflection-point method, the burning rate of the 14.9% methanol is lower than the baseline over the entire tested pressure range except at pressures below 5 MPa. For the peak-pressure method, the burning rates of the 14.9% methanol mixture is higher than that of the baseline over the entire pressure range except near 10 MPa. This result implies methanol slows the burning of HAN mixtures up until the inflection point, but accelerates the burning after the inflection point. It is thought that the initial burning is limited by the vaporization of the methanol, which has a much lower heat of vaporization than water. Chang et al. suggest that as the methanol vaporizes, water and HAN droplets could become entrained and subsequently react in the two-phase region [20].

Using the peak-pressure method, the addition of the silica in the methanol/silica mixture appeared to somewhat diminish the effects of the methanol and return the burning rates closer to the baseline. However, the inflection point method showed that the additional silica further reduced the burning rates from the baseline except at a pressure near 10 MPa. It could be that the increased viscosity produced by the silica stabilizes and slows the burning surface, while the relatively low temperature at the burning surface caused by the methanol vaporization [20] prevents the silica from contributing any heat transfer or catalytic effects. If the silica is having this effect, the

combination of methanol and silica in aqueous HAN could prove to be a useful propellant with stable burning and lower flame temperatures.

5.2 Future Studies

The work presented in this thesis has brought a better understanding of the combustion of HAN-based propellants. Still, many questions remain about the complex nature of the combustion of HAN mixtures. Foremost is the question of what causes the difference between the peak-pressure and inflection point methods of determining the propellant sample burning rates. It is known that a significant pressure rise occurs after the propellant sample has visually appeared to have completed burning. However, the mechanism for this pressure rise is still unknown. A more-detailed analysis of the non-equilibrium chemistry and thermodynamics may provide insight into this problem.

Future work could aim to improve the repeatability of the preparation of the HAN-based propellant mixtures. Limited analysis shows possible discrepancies in the compositions of the baseline batches from which all other mixtures are created. Improvements may come from better control of the water evaporation process and prevention of the re-emulsion of water from the atmosphere.

Finally, high-speed camera burning rate measurements could be performed on aqueous HAN mixtures containing silica, titania, and methanol. This additional study should be done to verify the inflection points are valid representations of the end of the visual burning for particle-containing mixtures as was done with the baseline.

Furthermore, visual observation could provide evidence that the silica and titania nanoparticles stabilize the burning surface or aid in vapor nucleation.

REFERENCES

- [1] Sutton, G.P., and Biblarz, O., "Rocket Propulsion Elements," John Wiley & Sons, New York, 2001, pp. 259-263.
- [2] Edwards, T., "Liquid Fuels and Propellants for Aerospace Propulsion: 1903-2003," *Journal of Propulsion and Power*, Vol. 19, No. 6, 2003, pp. 1089-1107.
- [3] Sabourin, J., Risha, G., Yetter, R., "Combustion characteristics of nanoaluminum, liquid water, and hydrogen peroxide mixtures," *Combustion and Flame*, Vol. 154, No. 3, 2008, pp. 587-600.
- [4] Schmidt, E., and Wucherer, E., "Hydrazines vs. non-toxic propellants: where do we stand now?" *2nd Conference (International) on Green Propellants for Space Propulsion Proceedings*, ESA SP-557, Cagliari, Sardinia, Italy, 2004.
- [5] Sasse, R., "Analysis of Hydroxylammonium Nitrate Based Liquid Propellants," U.S. Army Ballistic Research Lab, BRL-TR-3154, Aberdeen Proving Ground, MD, 1990.
- [6] Vosen, S.R., "The burning rate of hydroxylammonium nitrate-based liquid propellants," *Symposium (International) on Combustion*, Vol. 22, Elsevier, 1989, pp. 1817-1825.
- [7] Vosen, S.R., "Concentration and Pressure Effects on the Decomposition Rate of Aqueous Hydroxylammonium Nitrate Solutions," *Combustion Science and Technology*, Vol. 68, No. 4-6, 1989, pp. 85-99.

- [8] Katsumi, T., Hori, K., Matsuda, R., "Combustion wave structure of hydroxylammonium nitrate aqueous solutions," *The 46th AIAA/ASME/SAE/ASEE Joint Propulsion Conf. and Exhibit*, AIAA Paper 2010-6900, 2010.
- [9] Kondrikov, B., Annikov, V., Egorshv, V.Y., "Burning of hydroxylammonium nitrate," *Combustion, Explosion and Shock Waves*, Vol. 36, No. 1, 2000, pp. 135-145.
- [10] Wucherer, E., Christofferson, S., and Reed, B., "Assessment of high performance HAN-monopropellants," *36TH AIAA/ASME/SAE/ASEE Joint Propulsion Conference and Exhibit*, AIAA Paper 2000-3872, 2000.
- [11] Kuo, B., "A study on the electrolytic decomposition of HAN-based propellants for microthruster applications," Master's Thesis, The Pennsylvania State University, State College, PA, 2010.
- [12] Amrousse, R., Katsumi, T., Itouyama, N., "New HAN-based mixtures for reaction control system and low toxic spacecraft propulsion subsystem: Thermal decomposition and possible thruster applications," *Combustion and Flame*, Vol. 162, No. 6, 2015, pp. 2686-2692.
- [13] Schmidt, E.W., "Hydroxylammonium Nitrate Compatibility Tests with Various Materials-A Liquid Propellant Study," U.S. Army Ballistic Research Lab, BRL-CR-636, Aberdeen Proving Ground, MD, 1990.
- [14] Katsumi, T., Kodama, H., Matsuo, T., "Combustion characteristics of a hydroxylammonium nitrate based liquid propellant. Combustion mechanism and

- application to thrusters," *Combustion, Explosion, and Shock Waves*, Vol. 45, No. 4, 2009, pp. 442-453.
- [15] Yi-Ping Chang, and Kuo, K., "Assessment of combustion characteristics and mechanism of a HAN-based liquid monopropellant," *37th Joint Propulsion Conference and Exhibit*, AIAA Paper 2001-3272, 2001.
- [16] McBratney, W.F., "Burning rate data, LGP 1845," U.S. Army Ballistics Research Lab, ARBRL-MR-03128, Aberdeen Proving Ground, MD, 1981.
- [17] McBratney, W., and Vanderhoff, J., "High Pressure Windowed Chamber Burned Rate Determination of Liquid Propellant XM46," U.S. Army Research Lab, ARL-TR-442, Aberdeen Proving Ground, MD, 1994.
- [18] Cruice, W.J., "Classification of Liquid Gun Propellants and Raw Materials for Transportation and Storage." U.S. Army Ballistic Research Lab, ARBRL-CR-00454, Aberdeen Proving Ground, MD, 1981.
- [19] Klein, N., "Liquid Propellants for Use in Guns-A Review," U.S. Army Ballistic Research Lab, BRL-TR-2641, Aberdeen Proving Ground, MD, 1985.
- [20] Yi-Ping Chang, Josten, K., Kuo, K., "Combustion Characteristics of Energetic HAN/Methanol-Based Monopropellants," *38th AIAA/ASME/SAE/ASEE Joint Propulsion Conference and Exhibit*, AIAA Paper 2002-4032, 2002.
- [21] Sasse, R.A., Davies, M.A., Fifer, R.A., "Density of Hydroxylammonium Nitrate Solutions," U.S. Army Ballistic Research Lab, BRL-MR-3720, Aberdeen Proving Ground, MD, 1988.

- [22] Decker, M., Freedman, E., Klein, N., "Titrimetric Analysis of Han-Based Liquid Propellants," U.S. Army Ballistic Research Lab, BRL-TR-2907, Aberdeen Proving Ground, MD, 1988.
- [23] Vosen, S.R., "Hydroxylammonium nitrate-based liquid propellant combustion-interpretation of strand burner data and the laminar burning velocity," *Combustion and Flame*, Vol. 82, No. 3, 1990, pp. 376-388.
- [24] Oberle, W.F., and Wren, G.P., "Burn rates of LGP 1846 conditioned ambient, hot, and cold," U.S. Army Ballistic Research Lab, BRL-TR-3287, Aberdeen Proving Ground, MD, 1991.
- [25] Zhu, D., and Law, C., "Aerothermochemical studies of energetic liquid materials: 1. Combustion of HAN-based liquid gun propellants under atmospheric pressure," *Combustion and Flame*, Vol. 70, No. 3, 1987, pp. 333-342.
- [26] Lee, T., Tseng, L., and Faeth, G., "Separated-flow considerations for pressure-atomized combusting monopropellant sprays," *Journal of Propulsion and Power*, Vol. 6, No. 4, 1990, pp. 382-391.
- [27] Van Dijk, C., and Priest, R., "Thermal decomposition of hydroxylammonium nitrate at kilobar pressures," *Combustion and Flame*, Vol. 57, No. 1, 1984, pp. 15-24.
- [28] Shaw, B., and Williams, F., "A model for the deflagration of aqueous solutions of hydroxylammonium nitrate," *Symposium (International) on Combustion*, Vol. 24, Elsevier, 1992, pp. 1923-1930.

- [29] Lee, H., and Litzinger, T.A., "Chemical kinetic study of HAN decomposition," *Combustion and Flame*, Vol. 135, No. 1, 2003, pp. 151-169.
- [30] Wickham, D., Cook, R., de Voss, S., "Soluble nano-catalysts for high performance fuels," *Journal of Russian Laser Research*, Vol. 27, No. 6, 2006, pp. 552-561.
- [31] Risha, G.A., Son, S.F., Yetter, R., "Combustion of nano-aluminum and liquid water," *Proceedings of the Combustion Institute*, Vol. 31, No. 2, 2007, pp. 2029-2036.
- [32] McCown, K.W., and Petersen, E.L., "Effects of nano-scale additives on the linear burning rate of nitromethane," *Combustion and Flame*, Vol. 161, No. 7, 2014, pp. 1935-1943.
- [33] McCown III, K.W., Demko, A.R., and Petersen, E.L., "Experimental techniques to study linear burning rates of heterogeneous liquid monopropellants," *Journal of Propulsion and Power*, Vol. 30, No. 4, 2014, pp. 1027-1037.
- [34] McCown III, K.W., and Petersen, E.L., "Effects of Methanol and Fumed Silica on Linear Burning Rates of Aqueous Hydroxylammonium Nitrate," *International Journal of Energetic Materials and Chemical Propulsion*, Vol. 14, No. 1, 2015, pp. 1-12.
- [35] Homan-Cruz, G.D., McCown III, K.W., and Petersen, E.L., "Effects of Nano-scale Additives and Methanol on the Linear Burning Rates of Aqueous HAN Solutions," *50th AIAA/ASME/SAE/ASEE Joint Propulsion Conference*, AIAA Paper 2014-3566, 2014.

- [36] Stahl, J., Homan-Cruz, G., and Petersen, E., "Comparison of Liquid Monopropellant Burning Rates from Pressure Data and High-Speed Video," *9th U.S. National Combustion Meeting*, Combustion Institute, 2015.
- [37] Warren, W.C., "Experimental Techniques for the Study of Liquid Monopropellant Combustion," Master's Thesis, Texas A&M University, College Station, TX, 2012.

APPENDIX A

To verify the method of preparing 82.4 wt% HAN baseline solutions by evaporating water from the purchased 24 wt% HAN solution, a density study was performed. A Fisherbrand Finnpiptette II 1-5 mL volumetric pipette was used to measure out and deposit 1 mL samples of aqueous HAN onto the Ohaus ARA520 scale. The density is then calculated as the mass measured by the scale divided by 1 mL. The supplier provided 24 wt% HAN, the concentrated baseline of 82.4 wt% HAN, and a concentrate 90 wt% HAN batch were tested in this way five times each, and the resulting densities were averaged. Figure 15 shows the results of these density measurements compared with the second-order polynomial regression developed by Sassé [5, 21] and the results reported by Vosen [7]

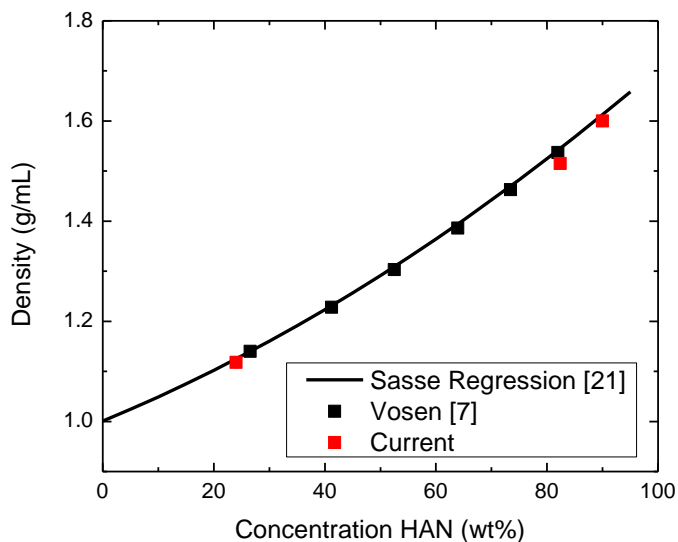


Figure 15. Density measurement results from the current study compared to the regression developed by Sassé et al. [21] and the results reported by Vosen [7].

APPENDIX B

The following tables contain the chamber pressure and linear burning rate data for all propellant mixtures measured in the current thesis.

Table B1. Average chamber pressures and linear burning rates for aqueous 82.4 wt% HAN baseline using peak-pressure method [34] and re-measured with the inflection point method.

Batch	Chamber Pressure (MPa)	Peak-Pressure Burning Rate (mm/s)	Inflection Point Burning Rate (mm/s)
	3.13	7.50	38.60
	3.45	11.53	82.09
	3.97	20.54	98.84
	4.16	26.40	87.73
	4.19	28.20	138.68
	4.56	39.20	128.81
	4.88	47.51	260.75
	5.26	60.23	157.25
	6.24	60.32	209.43
	7.27	58.86	166.19
McCown [34]	8.33	56.71	229.47
	8.96	53.55	278.66
	9.05	56.11	227.48
	10.54	47.43	204.31
	12.27	48.92	207.50
	14.28	46.89	190.14
	16.60	40.93	209.59
	18.55	39.24	167.79
	20.87	38.12	174.49
	9.64	53.88	179.27
	12.89	49.48	180.15
	10.61	46.53	148.53

Table B1. Continued

Batch	Chamber Pressure (MPa)	Peak-Pressure Burning Rate (mm/s)	Inflection Point Burning Rate (mm/s)
Oct-2-14	5.07	-	136.73
	6.14	-	197.14
	7.06	-	215.44
	8.18	-	230.64
	9.06	-	229.01
	10.68	-	238.23
	11.95	-	232.16
	13.34	-	211.88
	14.70	-	217.79
Oct-22-14	5.06	-	201.57
	5.71	-	234.77
	6.59	-	280.05
	7.81	-	285.36
	9.17	-	251.88
	11.84	-	206.03

Table B2. Average chamber pressures and linear burning rates for HAN baseline with 1 wt% silica additive using peak-pressure method and re-measured with the inflection point method.

Chamber Pressure (MPa)	Peak-Pressure Burning Rate (mm/s)	Inflection Point Burning Rate (mm/s)
3.13	64.41	129.19
3.83	78.23	171.29
4.55	87.66	233.16
5.26	79.33	226.39
5.95	74.83	238.78
7.38	68.49	190.77
9.13	61.90	171.28
10.91	58.04	200.32
12.99	54.39	185.82
15.84	51.32	190.35
18.34	49.13	159.45
20.76	46.40	189.43

Table B3. Average chamber pressures and linear burning rates for baseline HAN with 3 wt% silica additive using peak-pressure method and re-measured with the inflection point method.

Chamber Pressure (MPa)	Peak-Pressure Burning Rate (mm/s)	Inflection Point Burning Rate (mm/s)
3.33	108.03	235.96
3.76	109.06	280.57
4.62	105.42	272.51
5.00	107.66	221.93
5.94	94.11	269.93
6.80	89.21	280.33
7.56	74.22	274.58
8.90	74.76	261.32
10.22	65.44	243.14
13.05	52.87	190.85
14.45	50.52	170.49
15.67	52.07	157.42
18.40	45.89	151.24
21.26	47.21	183.89

Table B4. Average chamber pressures and linear burning rates for baseline HAN with 1 wt% titania additive using peak-pressure method and re-measured with the inflection point method.

Chamber Pressure (MPa)	Peak-Pressure Burning Rate (mm/s)	Inflection Point Burning Rate (mm/s)
3.12	49.82	165.42
3.84	66.21	106.90
4.56	75.47	192.08
5.29	68.96	217.15
6.23	66.89	194.43
7.08	64.94	180.52
8.10	61.41	231.47
9.85	56.74	257.60
11.57	53.98	206.86
13.99	51.38	183.84
16.53	49.18	167.34
18.75	45.65	204.64
20.78	44.21	168.14

Table B5. Average chamber pressures and linear burning rates for baseline HAN with 3 wt% titania additive using peak-pressure method and re-measured with the inflection point method.

Chamber Pressure (MPa)	Peak-Pressure Burning Rate (mm/s)	Inflection Point Burning Rate (mm/s)
3.11	40.78	82.12
3.91	56.33	116.63
4.54	70.64	162.75
5.19	73.80	166.43
5.71	72.12	198.55
6.75	71.71	250.32
8.63	63.88	246.97
10.31	57.83	236.52
12.31	50.48	179.90
14.64	51.26	158.86
18.90	47.00	147.65

Table B6. Average chamber pressures and linear burning rates for baseline HAN with 14.9 wt% methanol using peak-pressure method and re-measured with the inflection point method.

Chamber Pressure (MPa)	Peak-Pressure Burning Rate (mm/s)	Inflection Point Burning Rate (mm/s)
3.12	103.92	127.70
3.44	108.17	131.47
4.14	105.19	168.59
4.84	99.65	143.65
5.77	80.08	126.09
6.69	75.44	119.30
7.65	62.63	76.11
8.71	55.06	56.86
9.89	51.26	55.01
10.75	48.44	-
11.22	54.30	92.87
11.75	68.92	94.78
12.13	85.61	105.09
12.43	97.68	133.81
13.89	102.12	143.66
15.06	97.77	172.06
16.10	101.49	143.53
17.17	80.79	177.92
18.16	67.43	140.54
19.36	49.93	76.43
21.55	49.05	91.53

Table B7. Average chamber pressures and linear burning rates for baseline HAN with 14.9 wt% methanol and 1 wt% silica additive using peak-pressure method and re-measured with the inflection point method.

Chamber Pressure (MPa)	Peak-Pressure Burning Rate (mm/s)	Inflection Point Burning Rate (mm/s)
3.08	8.85	8.85
3.60	13.55	14.30
4.10	25.30	31.23
4.58	31.27	34.94
5.43	37.31	41.19
6.16	44.53	48.72
7.49	63.47	72.53
8.62	70.73	80.51
8.90	64.28	83.53
9.65	60.06	78.80
10.36	48.77	82.56
10.36	52.38	89.46
11.00	44.46	84.01
11.08	43.45	79.66
12.29	57.22	84.18
13.58	66.13	77.26
14.99	49.60	59.57
16.39	40.44	47.61
17.58	41.78	45.83
18.51	46.59	54.44
20.20	51.07	70.86